Cell, Vol. 103, 655–665, November 10, 2000, Copyright ©2000 by Cell Press

Solution Structure of the Interacting Domains of the Mad–Sin3 Complex: Implications for Recruitment of a Chromatin-Modifying Complex

Kurt Brubaker,* Shaun M. Cowley,‡ Kai Huang,*† Lenora Loo,‡ Gregory S. Yochum,§ Donald E. Ayer,§ Robert N. Eisenman,‡ and Ishwar Radhakrishnan*‖

*Department of Biochemistry, Molecular Biology, and Cell Biology
†Structural Biology NMR Facility
Northwestern University
Evanston, Illinois 60208
‡Division of Basic Sciences
Fred Hutchinson Cancer Center
Seattle, Washington 98109
§Huntsman Cancer Institute
University of Utah
Salt Lake City, Utah 84112

Summary

Gene-specific targeting of the Sin3 corepressor complex by DNA-bound repressors is an important mechanism of gene silencing in eukaryotes. The Sin3 corepressor specifically associates with a diverse group of transcriptional repressors, including members of the Mad family, that play crucial roles in development. The NMR structure of the complex formed by the PAH2 domain of mammalian Sin3A with the transrepression domain (SID) of human Mad1 reveals that both domains undergo mutual folding transitions upon complex formation generating an unusual left-handed four-helix bundle structure and an amphipathic α helix, respectively. The SID helix is wedged within a deep hydrophobic pocket defined by two PAH2 helices. Structure-function analyses of the Mad–Sin3 complex provide a basis for understanding the underlying mechanism(s) that lead to gene silencing.

Introduction

The recruitment of coactivators or corepressors by DNA-bound transcription factors has emerged as a common, highly conserved mechanism of transcriptional regulation (Ptashne and Gann, 1997). Transcription factor–mediated recruitment permits gene-specific targeting of coactivator/corepressor complexes with intrinsic or associated chromatin-modifying or chromatin-remodeling activities. A particularly well-characterized example is the Sin3 corepressor complex, one of two major corepressor complexes described to date, which is highly conserved from yeast to humans (Knoepfler and Eisenman, 1999). Sin3 appears to function as a large protein scaffold capable of multiple protein–protein interactions. On one hand Sin3 interacts with class I histone deacetylases (HDAC1 and HDAC2) and presumed accessory proteins such as RbAp48, SAP30, and SAP18 (Hassig et al., 1997; Laherty et al., 1997; Zhang et al., 1997). On the other hand, Sin3 associates with a surprisingly wide range of DNA binding transcription factors, including the nuclear hormone receptors (through the N-CoR and SMRT corepressors) (Alland et al., 1997; Heinzel et al., 1997; Nagy et al., 1997), PLZF (David et al., 1998), MeCP2 (Jones et al., 1998; Nan et al., 1998), Ski (Nomura et al., 1999), p53 (Murphy et al., 1999), Ikaros and Aiolos (Koipally et al., 1999), REST/NRSF (Naruse et al., 1999; Grimes et al., 2000), MNF-β (Yang et al., 2000), and the Mad family of Max binding bHLH-Zip transcriptional repressors (Ayer et al., 1995; Schreiber-Agus et al., 1995). The activities of these proteins and their ability to interact with Sin3 are thought to be crucial for cell proliferation and differentiation (for recent reviews see Ayer, 1999; Knoepfler and Eisenman, 1999; Ahringer 2000; and Ng and Bird, 2000).

The nature and possible regulation of the specific interaction between transcription factors and Sin3 is of great interest. For nuclear hormone receptors, the interaction with N-CoR/SMRT is hormone regulated (Chen and Evans, 1995; Hörlein et al., 1995) while for "dedicated" repressors such as the Mad protein family, the association appears to be constitutive. In the case of the Mad proteins, all four family members (Mad1, Mxi1, Mad3, and Mad4) and the related repressor, Mnt (or Rox) contain an ~30-residue, N-terminally located segment known as the Sin3 interaction domain, or SID, which is both necessary and sufficient for Sin3 association and for transcriptional repression (Ayer et al., 1995; Schreiber-Agus et al., 1995; Hurlin et al., 1997). Deletion or specific mutation of the SID abrogates Mad repression as well as its growth inhibitory functions. Furthermore, the Mad SID is capable of conferring repression activity when fused to a heterologous DNA binding domain (Ayer et al., 1996). Helical wheel analysis and circular dichroism (CD) studies of the Mad SID suggested that it had the potential to form an amphipathic α helix. Mutational analyses further demonstrated that a cluster of residues on the apolar face of the helix is essential for interaction with mammalian Sin3A (mSin3A) (Eilers et al., 1999).

Sin3 interacts with many proteins in the complex through four imperfect repeats of ~100 residues known as paired amphipathic helix (PAH) domains. The PAH domains, which were each suggested to be organized into two α helices separated by a flexible spacer region (Wang et al., 1990), are among the most evolutionarily conserved regions of the large Sin3 proteins (100–170 kDa). Indeed, these domains are important for Sin3 function as a corepressor, most likely through their independent associations with various repressors and other associated proteins. For example, PAH2 is both necessary and sufficient for interaction with the Mad proteins (Ayer et al., 1995, 1996; Schreiber-Agus et al., 1995) as well as with a newly discovered Sin3-interacting protein, Pf1 (G. S. Y. and D. E. A., unpublished data). PAH1 on the other hand, associates with N-CoR (Alland et al., 1997; Heinzel et al., 1997; Laherty et al., 1998) and PLZF (David

‖To whom correspondence should be addressed (e-mail: i-radhakrishnan@northwestern.edu).

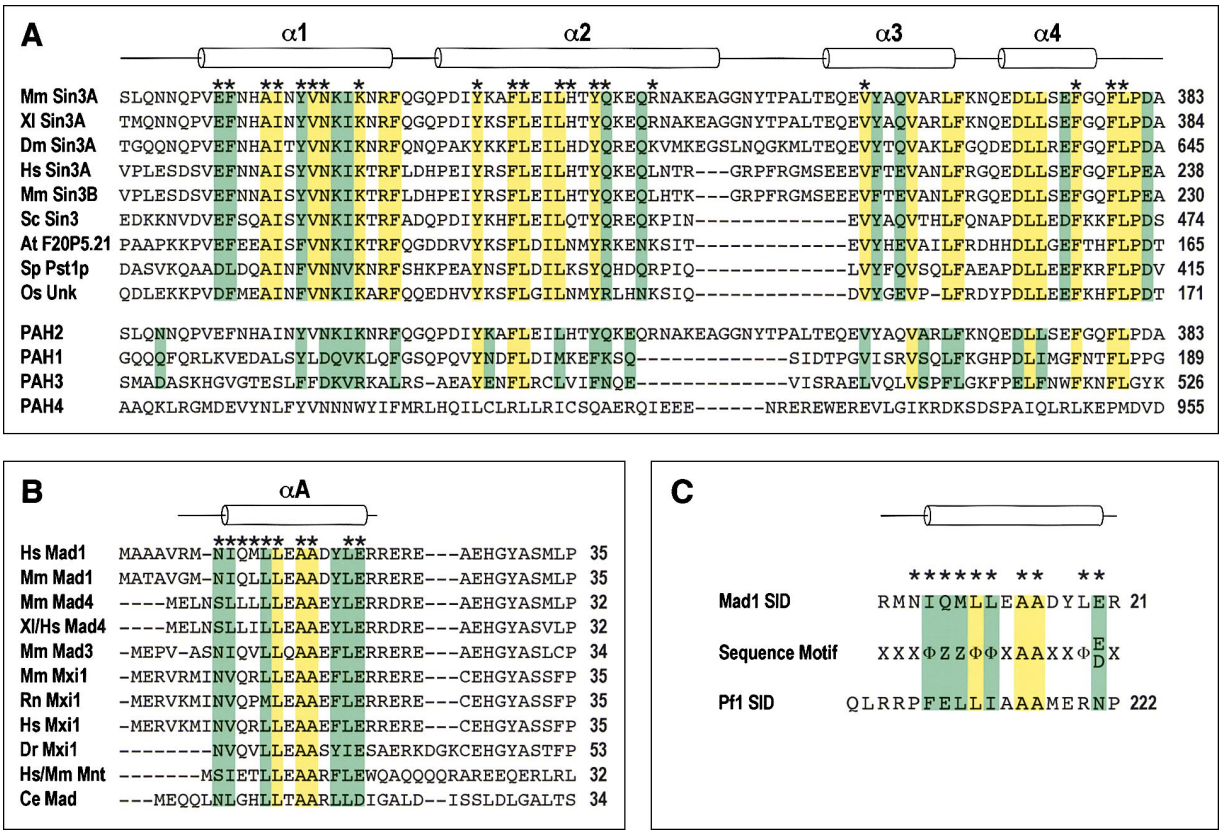

Figure 1. Multiple Sequence Alignments of PAH and SID Domains

CLUSTAL W generated alignments of (A) the PAH2 domain of putative Sin3 homologues (*top*), the PAH domains of mSin3A (*bottom*), and (B) the PAH2-interacting SID domains from various species (prefix abbreviations: Hs: *H. sapiens*; Mm: *M. musculus*; Xl: *X. laevis*; Dm: *D. melanogaster*; Ce: *C. elegans*; Rn: *R. norvegicus*; and Dr: *D. rerio*). (C) Pairwise sequence alignments of minimal SID domains from Mad1 and Pf1 guided by the PAH2-interaction motif. Sequence identities (yellow) and similarities (green) are highlighted. Stars identify interfacial residues (i.e., those that contribute more than 1% and 5% of the interfacial area in the respective proteins) in the PAH2–SID complex. The sequence motif in (C) is given in the standard one-letter code for amino acids; ϕ = any bulky hydrophobic residue; X = any non-proline residue; and Z = any hydrophobic or polar/charged residue with a significant aliphatic component.

et al., 1998), while PAH3 binds the SAP30 protein (Laherty et al., 1998).

While previous work on repressor–Sin3 corepressor interactions localized functionally important regions and provided hints regarding their structure, details of these important interactions were largely unknown. Here, we describe a high-resolution structure of the Mad1 SID bound to the PAH2 domain of mSin3A determined by NMR (nuclear magnetic resonance) methods. We also present mutational studies of mSin3A that confirm many of the specific interactions predicted from the NMR structure. Finally, we show that an unrelated Sin3-interacting protein, Pf1, with an interaction domain distinct from the Mad family SID, is likely to interact with PAH2 in a manner closely resembling Mad1 SID.

Results

Structure Determination

Members of the Mad family as well as the closely related Mnt/Rox proteins specifically bind the PAH2 domain of Sin3 (Figure 1A). For structural studies, this region corresponding to residues 295–383 of mSin3A was expressed as a recombinant protein in *E. coli*. To assess the conformational features of this domain, we recorded a ^{1}H-^{15}N correlated NMR spectrum (Figure 2A). Backbone amide proton resonances in the spectrum are well dispersed, characteristic of a folded protein. Closer inspection reveals that the number of backbone amide correlations far exceeds the number expected (84) for the 89-residue protein. Indeed, many well-resolved correlations occur in pairs indicative of at least two distinct backbone conformations that interconvert slowly on the time scale of the NMR experiment. The conformational heterogeneity persists over the pH range 4.5–6.0 at 27°C and also over the temperature range 15°C–35°C at pH 6.0 with only moderate changes in the relative populations of the two conformers. In addition, the spectrum is dominated by intense correlations in the 7.5–8.5 ppm region of the ^{1}H spectrum characteristic of unstructured, flexible regions in the protein. Indeed, the measured {^{1}H}-^{15}N nuclear Overhauser effects (NOEs) for backbone amides follow a distribution quite distinct from that of a fully folded domain with more than 50% of the residues exhibiting values less than 0.6 (global average = 0.5 ± 0.4). These conformational features do not appear to be

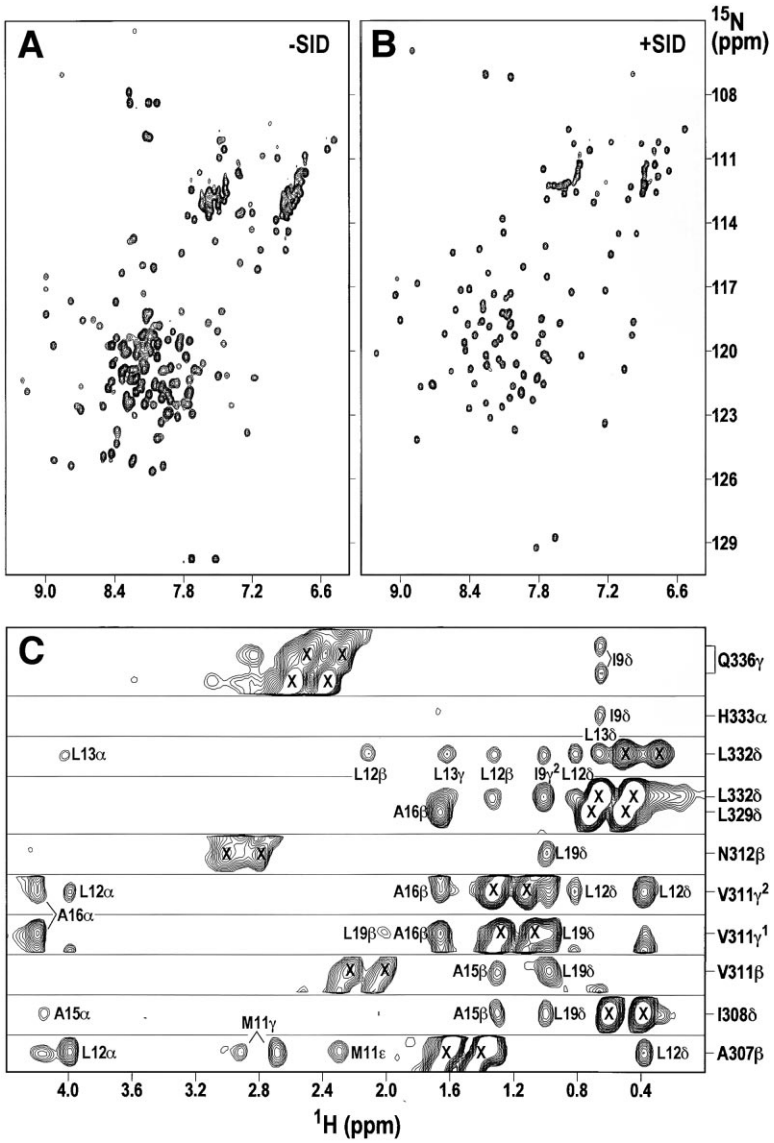

Figure 2. ^{1}H-^{15}N-Correlated Spectra of PAH2 and Intermolecular NOEs in the PAH2–SID Complex

Heteronuclear correlation maps of (A) free PAH2 and (B) PAH2 in the presence of an equivalent amount of SID. (C) Selected strips from a 3D ^{13}C-filtered, ^{13}C-edited NOESY spectrum depicting intermolecular NOEs. Incompletely suppressed signals from ^{13}C-bound protons (diagonal peaks) are denoted by an "X".

an artifact of the construct since a longer construct comprising residues 273–410 of mSin3A also exhibits similar properties (data not shown). Collectively, these results suggest that the PAH2 domain of full-length mSin3A may not be fully folded and that it might exist in at least two distinct, stable conformations when not bound to another protein. How these two conformations differ from each other remains to be elucidated.

The Mad proteins, particularly those from higher organisms, share sequence similarity that extends over 30 residues at the N terminus (Figure 1B). However, only residues 8–20 of human Mad1 appear to be necessary and sufficient for interaction with Sin3 in vitro as well as in vivo (Eilers et al., 1999). A synthetic peptide corresponding to residues 6–21 of Mad1 (henceforth designated SID) binds to mSin3A PAH2 with comparable affinity as another peptide corresponding to residues 1–35 of Mad1 ($K_D \sim$29 nM and 15 nM, respectively) in isothermal titration calorimetry (ITC) measurements. Both peptides bind to PAH2 with 1:1 stoichiometry. Structural analysis of free SID using NMR spectroscopy was not feasible owing to peptide aggregation at the concentrations ($>$0.5 mM) required for such studies, although CD spectra of a closely related SID peptide had suggested the absence of any intrinsic secondary structure in aqueous solution in the free state (Eilers et al., 1999).

The ^{1}H-^{15}N correlated spectrum of the PAH2 construct (mSin3A residues 295–383) in the free state is in complete contrast to the one obtained in the presence of an equivalent amount of the SID peptide (Mad1 residues 6–21) where only one correlation is seen for every residue (Figure 2B). Moreover, the resonance intensities are relatively uniformly distributed, only 20% of the residues exhibit $\{^{1}H\}$-^{15}N NOEs less than 0.6 (global average $=$ 0.67 $\pm$ 0.21), and the amide protons are well dispersed, indicative of a unique, folded conformation for PAH2 in the presence of the Mad1 SID. Intermolecular NOEs suggest that these profound spectral changes are caused by direct physical interactions between the two entities (Figure 2C).

Table 1. NMR Structure Determination Statistics

Constraint Statistics	
Distance constraints	1612
Intraresidue	694
Sequential ($\|i - j\| = 1$)	359
Medium-range ($1 < \|i - j\| \leq 4$)	310
Intramolecular long-range ($\|i - j\| > 4$)	168
Intermolecular	81
Torsion angle constraints	198 [73 ϕ, 73 ψ, 52 χ^1]
$^3J_{H^N H^\alpha}$ coupling constants	72
Structure Statistics (14 Structures)	
Constraint satisfaction	
RMS diff. for distance constraints	0.018 ± 0.001 Å
Distance constraint violations (>0.2 Å)	1.71 ± 0.99
RMS diff. for torsion angle constraints	0.34 ± 0.06°
Torsion angle violations (>5°)	0.14 ± 0.36
RMS diff. for coupling constants	0.47 ± 0.02 Hz
Coupling constant violations (>1 Hz)	0.93 ± 0.92
Deviations from ideal covalent geometry	
Bond lengths	0.0039 ± 0.0001 Å
Bond angles	0.56 ± 0.02°
Impropers	0.40 ± 0.02°
Ramachandran plot statistics	
Residues in most favored regions	85.6%
Residues in allowed regions	12.9%
Residues in disallowed regions	1.5%
RMS Deviations from Minimized, Average Structure	
All atoms	2.57 Å
All atoms (excl. residues 295–301 of PAH2)	1.47 Å
Backbone atoms (N, C^α, C′)	
All residues	2.09 Å
All residues (excl. residues 295–301 of PAH2)	0.76 A
Helices (α1, α2, α3, α4, and αA	0.52 Å

The exceptionally high quality of the NMR spectra of the PAH2–SID complex permitted a high-resolution structural characterization. Structural data in the form of interproton distances, three-bond scalar coupling constants, and torsion angles were measured to calculate and refine three-dimensional structures of the complex (Table 1). Fourteen structures (as well as the energy-minimized, average structure) with backbone conformations predominantly in favorable regions of ϕ-ψ space and no serious constraint violations (Table 1) were selected for detailed analysis (Figure 3A).

Overall Structure of the Complex

The PAH2 domain of mSin3A adopts a left-handed, up-and-down, four-helix bundle structure with residues in all four helices as well as in the turn regions defining a compact structural domain with an extensive hydrophobic core (Figures 3 and 4). Helices α1 and α2 form a deep hydrophobic pocket, which constitutes the primary interaction surface for the Mad1 SID peptide. The SID peptide forms an amphipathic α helix in the complex and interacts with PAH2 mainly through the apolar surface of the helix.

Structure of the PAH2 Domain

An unusual feature of the PAH2 four-helix bundle is the widely differing lengths of the constituent helices, with helices α1, α2, α3, and α4 comprising 16, 24, 11, and 8 residues, respectively (Figure 3B). Helix α1 extends from residue Val302 to Arg317, while the α2, α3 and α4 helices span residues Pro322–Ala345, Glu355–Leu365, and Glu370–Gly377, respectively. The α1 and α2 helices are approximately coplanar and pack against each other at an unusual ~45° angle, which precludes efficient packing between these helices except at one end (i.e., the C terminus of helix α1 with the N-terminal portion of α2). By contrast, helices α2 and α3, and α3 and α4 pack at angles of ~10° and ~16°, respectively, making contacts with each other throughout their lengths (Figure 3B). The α2, α3, and α4 helices thus pack approximately parallel to each other while helix α1 projects away from this "core" and toward the solvent. However, this does not preclude the C-terminal region of α1 to engage in packing interactions with α4 and indeed the two helices interact in a "knobs-into-holes" type pattern at an angle of ~22°.

The linker regions connecting α1–α2, α2–α3, and α3–α4 helices as well as the region following the α4 helix are each distinguished by four-residue β turns involving residues Phe318–Gln321, Ala345–Asn348, Phe366–Gln369, and Gln378–Pro381. The measured {^{1}H}-^{15}N NOE values for these residues (with the exception of Ala345–Asn348) are comparable (0.7 to 0.8) to those found in helical regions, implying no significantly enhanced flexibility for the polypeptide backbone at these positions compared to their helical counterparts. Indeed, several residues in the turn regions make key contributions to the hydrophobic core of the domain (Figure 4). In contrast, the C-terminal portion of the α2 helix as well as the turn and loop regions immediately following it (residues Gln339-Thr354) are characterized by distinctly low {^{1}H}-^{15}N NOE values (0.3 to 0.7) implying enhanced flexibility, which probably accounts for the greater variability in coordinate positions (Figure 3A). Residues 297–300

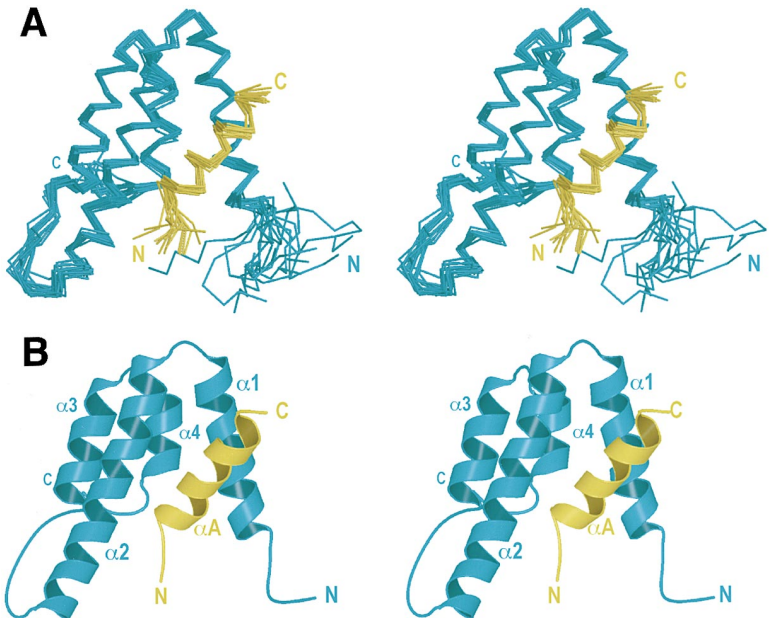

Figure 3. Solution Structure of the PAH2–SID Complex

Stereo views of (A) the C^{α} trace of a best-fit superposition (involving backbone atoms in helical regions) of the ensemble of 14 NMR structures and (B) a ribbon diagram of the energy-minimized, average structure. The PAH2 domain is colored cyan while the SID peptide is shown in yellow.

as well as residues 382–383 at the N and C termini also exhibit significantly diminished $\{^1H\}$-^{15}N NOE values (−0.3 to 0.4) and are similarly dynamically disordered. These regions constitute the least conserved segments of the PAH2 domain (Figure 1A).

The secondary structural elements of PAH2 enclose a fairly extensive hydrophobic core. Residues Ala307, Tyr310, Val311, and Ile314 in α1; Ile324, Tyr325, Phe328, Leu329, Ile331, Leu332, Thr334, and Tyr335 in α2; Val358, Tyr359, Val362, Ala363, and Leu365 in α3; Leu372, Leu373, and Phe376 in α4; and Phe318, Phe366, Phe379, and Leu380 in the turn regions define the primary hydrophobic core (Figure 4). Expectedly, these residues are also the most highly conserved residues in PAH2. Conspicuously absent from making significant contributions to the primary core are residues at the N terminus of the α1 helix. Indeed, this region is somewhat isolated from the remainder of the domain (Figure 4), perhaps accounting for the partial structural instability of PAH2 in the free state.

Structure of the SID Domain

CD spectra of a SID peptide (Mad1 residues 8–20) suggested the absence of any stable secondary structure in the free state (Eilers et al., 1999). Conceivably, upon binding to PAH2, the SID peptide undergoes significant conformational changes, forming a 12-residue amphipathic helix (αA) that extends from residue Ile9 to Glu20. The orientation of the SID αA helix is well defined relative to PAH2, consistent with the large number of intermolecular NOEs (81, Figure 2C) detected between the protein and the peptide. The side chain conformations are also

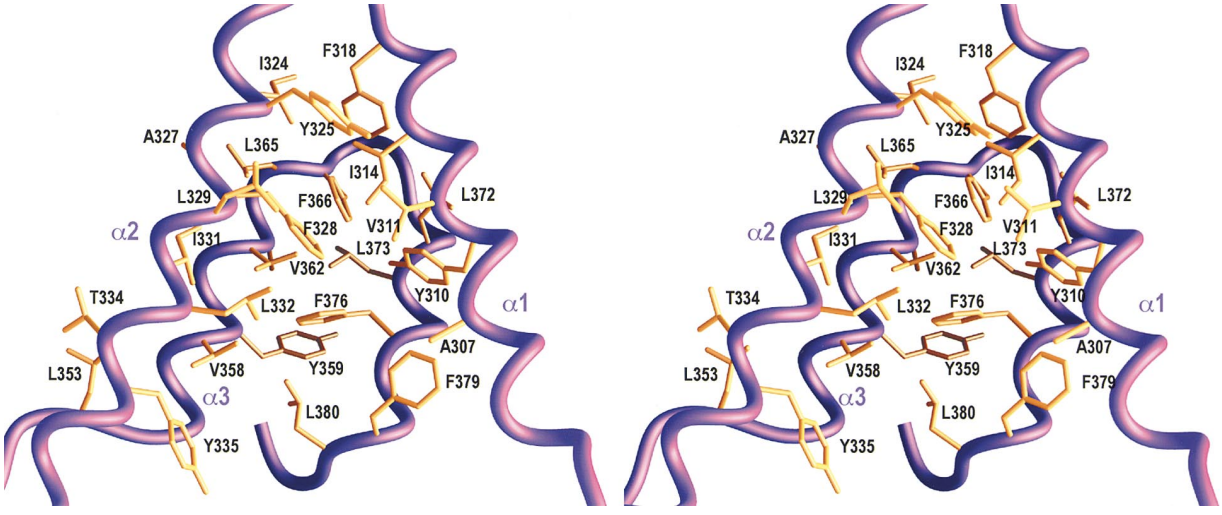

Figure 4. A Stereo View of the Hydrophobic Core of PAH2 in the PAH2–SID Complex

The side chains (gold) of residues belonging to α2, α3, α4 helices, and the C-terminal region of the α1 helix define the primary hydrophobic core.

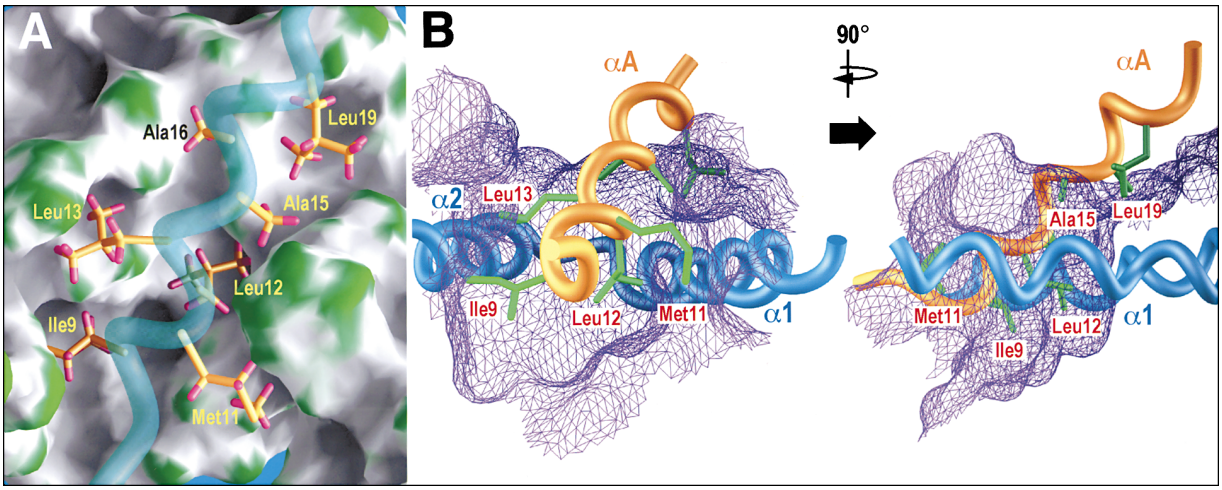

Figure 5. Interactions between PAH2 and SID

(A) A close-up view of the molecular surface of PAH2 is shown along with the interacting side chains (gold and magenta) of nonpolar residues of SID. The molecular surface is color coded according to curvature (gray: concave; white: flat; and green: convex). The SID peptide backbone (cyan) has been ghosted for clarity.

(B) Orthogonal views of the interacting helices of SID and PAH2 emphasizing the orientation of the αA helix (gold) relative to the α1 and α2 helices (blue). Apolar side chains (green) of SID and the molecular surface of PAH2 (purple mesh) that is within 2 Å of the molecular surface of SID are shown.

well defined, particularly for apolar residues that make extensive contacts with PAH2. The backbone and side chain conformations for residues preceding or following the αA helix are poorly defined in the NMR structures because of the absence of medium- and long-range NOEs involving these regions; the narrow resonance linewidths, however, suggest that these regions are unstructured in the complex.

The PAH2–SID Interface

Upon complex formation, both PAH2 and SID undergo mutual folding transitions. Together, the molecules bury over 1200 Å^2 of solvent-accessible surface (about 600 Å^2 in each protein). The intermolecular interface is formed by residues in the αA helix of SID and primarily the α1 and α2 helices of PAH2, although the α3 helix and the turn region following the α4 helix also contribute to some extent.

Poor packing between the α1 helix and the rest of the domain creates a deep binding pocket for the SID helix (Figure 5A). The floor of the pocket is defined by the side chains of Tyr335, Val358, Leu332, Phe328, Val311, Tyr310, Phe376, Ala307, Phe379, and Leu380 that also contribute significantly toward the hydrophobic core of the domain. The rim of the pocket on the other hand, is decorated by apolar, polar, as well as charged side chains belonging to the α1 and α2 helices including Phe304, Ile308, Asn312, Lys315, Tyr325, Leu329, His333, and Gln336 (Figure 6A). The apolar side chains Ile9, Met11, Leu12, and Leu13 located at the N terminus of the αA helix of SID, interact intimately and extensively with the floor of this pocket such that they appear to be an integral part of the hydrophobic core of the domain (Figure 5 and Figure 6A). Indeed, the N-terminal portion of the αA helix is deeply wedged between the PAH2 α1 and α2 helices (Figure 5B). Packing interactions between the α1 and α2 helices near the α1–α2 junction, however, forces the C-terminal portion of the αA helix to project out of this pocket although interactions with residues at the rim of the pocket are continued (Figure 5B). By virtue of their short side chains, Ala15 and Ala16 play a crucial role in allowing close contacts to be maintained between the two interacting surfaces. The alanine residues also facilitate the αA helix to cross over the α1 helix by engaging in "knobs-into-holes" type interactions (Figure 6A). The "hole" formed by Ala15, Ala16, and Leu19 of αA, for example, is occupied by Val311 of α1, while that formed by the side chains of Ile308, Val311, and Asn312 is filled by Leu19.

Noncovalent Interactions in the PAH2–SID Complex

To assess the individual contributions of interfacial residues toward the overall stability of the PAH2–SID complex, we have undertaken site-directed mutagenesis experiments. Three categories of residues in PAH2 were selected: (1) residues that contribute to the floor of the hydrophobic pocket, (2) residues forming the rim of this pocket, and (3) noninteracting, solvent-exposed residues (positive control). Mutations were introduced into full-length mSin3A, which was translated in vitro and assayed for binding to GST-Mad1 SID. Under the conditions of these assays, single-site category 1 and category 2 mutants Leu332Ala and Ile308Asp, respectively, both exhibit greatly diminished binding for SID (Figure 6B), consistent with the NMR structure. Leu332 makes van der Waals contacts with Leu12 and Leu13 of SID and also with other PAH2 residues in the hydrophobic core, consistent with its role in stabilizing the complex in addition to stabilizing the structure of the PAH2 domain. On the other hand, Ile308 engages in hydrophobic interactions with Ala15 and Leu19 of SID, thereby stabilizing the binary complex (Figure 6A). Predictably, category 1 and 2 dual-site combination mutants such as Ile308Asp,Val311Ala, Ile308Asp,Ala307Val and

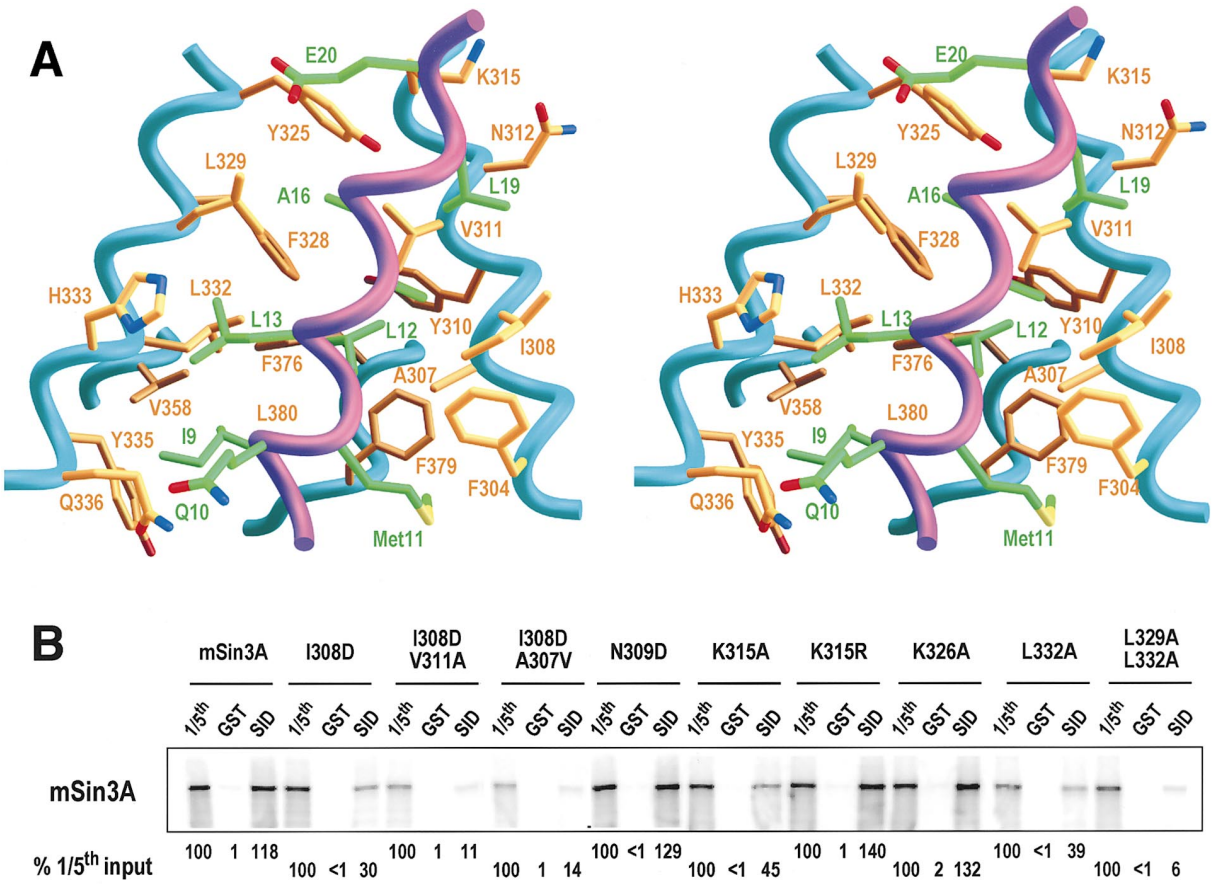

Figure 6. Noncovalent Interactions at the PAH2–SID Interface and Their Contributions to the Overall Stability of the Complex

(A) The side chains of PAH2 (gold) and SID (green) at the protein–protein interface are shown along with the respective polypeptide backbones (PAH2: cyan and SID: purple); noninteracting residues have been omitted for clarity.

(B) Binding activity of ^{35}S-methionine labeled wild-type or mutant mSin3A to GST-SID (Mad1 residues 1–27) or GST in a GST-pulldown assay. Bound proteins were separated via gel electrophoresis. The input lane (1/5th) represents 20% of the total protein added to the experiment. The amount of wild-type or mutant mSin3A bound to GST-SID or GST was quantitated using a phosphoimager and expressed as a percentage of the 1/5th input for each protein.

Leu332Ala,Leu329Ala exhibit more severe SID binding defects (Figure 6B) than the corresponding single-site mutants (i.e., Ile308Asp and Leu332Ala, respectively). By contrast, category 3 mutants Asn309Asp and Lys326Ala retain binding activity similar to wild-type levels (Figure 6B), consistent with their noninvolvement in any structure stabilizing role.

Mutational analyses identified a key intermolecular electrostatic interaction involving Lys315 and a glutamate residue (Glu20) in its immediate vicinity that is not well defined in the NMR structures owing to a lack of constraints between the respective side chains. The Lys315Ala mutant exhibits significantly reduced binding compared to wild type (Figure 6B), and whereas Lys315Glu mutant produces a similar effect (data not shown), the Lys315Arg mutant shows no loss of binding (Figure 6B), thus strongly implicating a positively charged residue at this position in an electrostatic interaction. Indeed, both Lys315 and Glu20 are highly conserved in PAH2 and SID (Figure 1B), confirming their important role in complex stabilization. Besides, Glu20 is the *only* charged residue that is highly conserved in SID.

A comprehensive mutational analysis had previously led to the definition of the boundaries of a minimal SID and also identified key residues that are involved in stabilizing the PAH2–SID complex (Eilers et al., 1999). The boundaries of the minimal SID (residues 8–20) determined by this study are virtually coincident with the endpoints of the SID αA helix (residues 9–20) determined from the NMR structure. Single-site mutations of residues on the apolar face of the amphipathic helix, including Leu12Glu, Ala15Asp, and Leu19Asp, exhibit significantly diminished binding compared to wild type, consistent with their role in mediating intermolecular interactions in the NMR structure. In contrast, mutations on the polar face of the helix, including Gln10Ala, Glu14Ala, and Asp17Ala, appear to have no effect consistent with their noninvolvement in intermolecular interactions.

Discussion

The solution structure of the mSin3A PAH2 domain bound to Mad1 SID provides a basis for understanding how repression domains of eukaryotic transcription fac-

tors target the closely related PAH domains of the Sin3 corepressor. Although previous analyses had suggested that the hydrophobic surface of the Mad1 SID helix was likely to interact with helical regions within mSin3A PAH2 (Ayer et al., 1996; Eilers et al., 1999), the present study defines the structural basis for the association at high resolution.

The NMR structural analyses reveal a number of features that are likely to be important for understanding the molecular basis of repression by the Mad–Sin3 repressor–corepressor complex. First, the interaction of the Mad1 SID with the mSin3A PAH2 domain results in the cooperative conversion of relatively disordered structures into a highly ordered cluster of helices (Figure 3). While SID folds from what appears to be a random coil conformation, PAH2 undergoes folding transitions from at least two distinct, but partially unfolded conformational states. This general type of mutual folding transitions has been described as "molecular Velcro" (O'Shea et al., 1993) and likely is an important factor in facilitating intimate interactions between the SID and PAH2 domains. Second, although earlier modeling of yeast and mammalian Sin3 proteins had suggested that the PAH domains each comprised two amphipathic helices (Wang et al., 1990; Ayer et al. 1995; Schreiber-Agus et al. 1995), our data establish that the PAH2 region involved in association with the Mad1 SID is more extensive, and in the fully folded state, consists of a compact four-helix bundle (Figure 1A and Figure 3). The four-helix bundle structure of the PAH2 domain appears to be a novel fold with no close relatives either in the FSSP (Holm and Sander, 1996) or the SCOP (Murzin et al., 1995) databases. Although this motif has been found in many structural contexts, bundles with a left-handed topology are relatively uncommon. Prominent examples of left-handed, four-helix bundles with an up-and-down topology, such as defined for the PAH2 region in this study, include cytochrome b_5 and the P/CAF and $TAF_{II}250$ bromodomains (Mathews et al., 1972; Dhalluin et al., 1999; Jacobson et al., 2000). None of these proteins, however, share significant structural similarity with the PAH2 domain. Given the high degree of sequence conservation of the PAH2 region (Figure 1A), we postulate that PAH2 domains of all known Sin3 proteins possess a very similar fold.

A striking feature of the four-helix bundle structure adopted by the PAH2 domain is the deep cleft formed by helices α1 and α2, which forms the interaction surface for the SID peptide (Figures 4, 5, and 6). The PAH2–SID interaction appears to be predominantly hydrophobic. We have used site-specific mutagenesis to show that a number of the noncovalent interactions between the SID and residues located on both the floor and the rim of the pocket are essential for efficient binding of the Mad1 SID to mSin3A in vitro (Figure 6B). Interestingly, the mutational analyses identified an unexpected electrostatic interaction between Lys315 in PAH2 and Glu20 in SID.

Sequence and Structural Requirements for PAH2-Interacting Domains

Because a number of transcription factors besides members of the Mad family target the PAH2 domain of Sin3, an important question is whether these other proteins employ the same mode of interaction with PAH2 as Mad. The NMR structure of the PAH2–SID complex, when considered in conjunction with mutational and sequence analysis, provides valuable insights into the sequence and structural requirements for PAH2-interacting domains. These considerations allow us to propose the following PAH2-interaction sequence motif: ϕ-Z-Z-ϕ-ϕ-X-Ala-Ala-X-X-ϕ-[Glu/Asp], where X is any nonproline residue, ϕ is any bulky hydrophobic residue, and Z is any hydrophobic or polar/charged residue with a significant aliphatic component in the side chain (i.e., Glu, Gln, Arg, or Lys). A sequence motif, though more restrictive than, for example, a profile-HMM (Hidden Markov Model), is nevertheless useful in identifying remote similarities because, with the exception of the closely related Mnt proteins, the Mad proteins do not share obvious sequence similarity with other PAH2-interacting proteins. The PAH2-interaction sequence motif allowed us to predict and test a Sin3 interaction domain of Pf1, a transcription factor recently shown to interact with mSin3A (G. S. Y. and D. E. A., unpublished data). The Pf1 SID amino acid sequence closely corresponds to this motif (Figure 1C), except at two positions: an arginine instead of a hydrophobic residue at position 11, and an asparagine instead of glutamate/aspartate at position 12. However, the hydrophobic residue at position 11 is relatively solvent exposed, suggesting that arginine, by virtue of its relatively long aliphatic side chain, might functionally substitute for a hydrophobic residue. Similarly, the asparagine might also functionally substitute to some extent for a negatively charged residue by participating in hydrogen bonding interactions with Lys315. We therefore synthesized a peptide corresponding to this domain and tested for binding activity in vitro. Pf1 SID produces a very similar effect on the NMR spectrum of PAH2 (data not shown) as Mad1 SID, implying that the interaction is specific and most likely similar in the two complexes. This is also suggested by the effects of various mSin3A mutations on the interaction with Pf1 SID (data not shown), which virtually mirror the effects observed with Mad1 SID in GST-pulldown assays (Figure 6B). In ITC measurements, the Pf1 SID peptide bound to PAH2, but with somewhat reduced affinity than Mad1 SID (580 nM versus 29 nM) because of the presumed differences in the intermolecular interactions in the two complexes (cf. above).

Using the same strategy however, we were unable to identify the PAH2-interaction domains in two other transcription factors proposed to target the PAH2 domain of Sin3: the neuronal restrictive silencer factor (NRSF/REST), and the myocyte nuclear factor (MNF-β) (Naruse et al., 1999; Grimes et al., 2000; Yang et al., 2000). Although further studies are required to definitively establish a direct interaction between these proteins and PAH2, it is possible that our understanding of the nuances of the PAH2-interaction motif is still incomplete or that these proteins bind to PAH2 through a motif different from the one found in Mad1. If the latter is true, the conformational heterogeneity of PAH2 in the free state assumes greater significance because it immediately suggests a mechanism whereby the domain can bind to unrelated sequences by adopting different folds, forming structurally distinct interaction surfaces.

Specificity of Protein–Protein Interactions Involving PAH Motifs

An intriguing feature of Sin3 recruitment by transcription factors is that although the first three PAH repeats share as much as 40% to 50% sequence similarity and, quite possibly, a highly similar fold, Sin3 binding proteins are capable of interacting only with a specific PAH repeat. For example, while Mad, Mnt/Rox, and Pf1 bind PAH2; N-CoR binds PAH1; and SAP30 binds PAH3 (Ayer, 1999; Knoepfler and Eisenman, 1999). Interestingly, sequence similarity among the PAH domains is not simply confined to residues that make up the hydrophobic core, but also includes residues that make up the putative protein–protein interaction surface. Indeed, at least three interfacial residues in the α2 helix, viz. Tyr325, Phe328, and Leu329, are invariant in the three PAH repeats, while several others in the α1 and α2 helices are highly conserved (Figure 1A). By contrast, the N-terminal region of the α1 helix exhibits the greatest sequence diversity among the three repeats, suggesting that the specificity of the interaction may reside within this region (Figure 1A). It is also possible that sequence similarities (as opposed to identities) at key positions within the domain may translate into subtle, but important differences in interior packing and sculpting of interfaces, leading to the observed differences in binding specificities.

The amphipathic helix structural motif has also been noted in the activation domains of transcriptional activators when bound to their cellular targets (Berk, 1999, and references cited therein). In common with the Mad SID αA helix, residues on the apolar face of the helical scaffold play key roles in complex stabilization. The conservation of this structural motif in transcriptional repression is intriguing because it creates the potential for cross-talk between positive and negative transcription regulatory networks, considering that these amphipathic helices are generally short (typically between 8–12 residues) and the interactions are mediated by only a few residues, limiting sequence diversity and, as a consequence, specificity. Clearly, additional structural and functional analyses will be required to fully understand the basis for specificity in recruitment of transcriptional coactivators and corepressors.

Experimental Procedures

Preparation of the mSin3A PAH2 Domain

The nucleotide sequence of the PAH2 domain, corresponding to residues 295–383 of mSin3A, was amplified via PCR and subcloned into the pET-24a(+) expression vector (Novagen). *E. coli* BL21(DE3) cells harboring the vector were grown at 37°C in LB media. Protein expression was induced using 1 mM isopropyl-1-thio-β-D-galactopyranoside (IPTG) when A_{600nm} was between 0.8 and 1. Cells were harvested 4 hr after induction. The cells were suspended in 50 mM Tris buffer (pH 8.5) containing 1 mM phenylmethylsulfonyl fluoride (PMSF), 1 μM leupeptin, 1 mM pepstatin, and 0.1% Triton X-100, lysed via sonication, centrifuged, and the supernatant loaded onto a Hi-Trap Q column (Amersham Pharmacia). The protein was eluted using 50 mM imidazole buffer (pH 6.5) containing 25 mM NaCl and subsequently purified to homogeneity via reverse-phase high pressure liquid chromatography (HPLC). The final yield of the protein was typically between 10 and 20 mg l^{-1} of culture. The identity of the protein (calculated molecular weight [mw] = 10,332.4; experimental mw = 10,333.0) was confirmed by electrospray ionization-mass spectrometry (ESI-MS).

Preparation of the Mad1 SID Domain

A hexadecapeptide corresponding to residues 6–21 of Mad1 (SID) was synthesized via automated methods (Genemed Synthesis). The synthetic peptide was capped at the N and C terminus by acetyl and amide protecting groups. The crude product was purified to homogeneity via reverse-phase HPLC. The identity of the peptide (calculated mw = 2007.1; experimental mw = 2006.7) was confirmed by ESI-MS.

Preparation of Uniformly Labeled PAH2

For NMR studies, PAH2 samples uniformly labeled with ^{15}N and/or ^{13}C isotopes were expressed and purified as described above, except cells were grown in M9 media containing ^{15}N-ammonium sulfate and D-glucose (or $^{13}C_6$-D-glucose) (Cambridge Isotopes), respectively, instead of LB. The extent of labeling was determined by ESI-MS (96% for ^{13}C, and 98% for ^{15}N).

PAH2–SID Complex Generation and NMR Sample Preparation

PAH2–SID complexes were generated by titrating increasing amounts of unlabeled SID peptide with ^{15}N- or ^{15}N,^{13}C-labeled PAH2. The progress of the titration was monitored by recording two-dimensional (2D) ^1H-^{15}N correlated spectra and noting the disappearance of correlations belonging to the "free" PAH2 species. At the conclusion of the titration, samples were lyophilized and resuspended in either 90% H_2O/10% D_2O or 100% D_2O. Sample concentrations for NMR experiments were typically 0.7–1.6 mM in 20 mM sodium phosphate buffer (pH 6.0) and 0.2% NaN_3.

NMR Spectroscopy

All NMR data were acquired on Varian Inova 500 and 600 MHz spectrometers at 27°C. NMR data processing and analysis were performed using Felix 98 software (Molecular Simulations) incorporating menu-driven interfaces developed in-house (Radhakrishnan et al., 1999). Backbone and side chain ^1H, ^{15}N, and ^{13}C resonances for PAH2 were assigned via double- and triple-resonance approaches (Bax and Grzesiek, 1993; Clore and Gronenborn, 1994). Backbone resonances were assigned from three-dimensional (3D) HNCA, HNCACB, CBCA(CO)NH, HNCO, and HCACO spectra while aliphatic side chain resonances were assigned from 3D ^{15}N-edited TOCSY, C(CO)NH-TOCSY, HCCH-COSY, and HCCH-TOCSY spectra. Aromatic side chain resonances were assigned from 2D (HB)CB(CGCD)HD, (HB)CB(CGCDCE)HE and 3D (HB)CBCG(CD)HD, (HC)C(C)CH-TOCSY spectra (Yamazaki et al., 1993; Löhr and Rüterjans, 1996). Forty-one out of fifty-three nondegenerate β-methylene proton resonances were assigned stereospecifically from an analysis of 3D HNHB and HACAHB spectra (Archer et al., 1991; Grzesiek et al., 1995). Backbone and side chain proton resonances for SID were assigned from an analysis of 2D ^{13}C- or ^{13}C,^{15}N-double-half-filtered NOESY and TOCSY spectra (Otting and Wüthrich, 1990). A detailed account of the NMR experiments and assignments will be given elsewhere.

In order to assess backbone flexibility, {^1H}-^{15}N heteronuclear NOE experiments were performed in duplicate (free) or quadruplicate (complex) at 14.1 T for backbone amides of PAH2 using 2D sensitivity-enhanced, water flip-back methods (Farrow et al., 1994).

Constraint Generation

A total of 1612 unique distance constraints were derived from 3D ^{15}N-edited NOESY (mixing time, τ_m = 80 ms), 3D aliphatic and aromatic ^{13}C-edited NOESY (τ_m = 60 ms), and 2D ^{13}C-double-half-filtered NOESY (τ_m = 100 ms) and 2D ^{13}C,^{15}N-double-half-filtered NOESY (τ_m = 80 ms) experiments. NOEs were assigned manually, but iteratively, with the help of the XPKASGN program. Cross peak intensities were calibrated against known interproton distances in α helices or aromatic rings. Distance constraints were assigned upper bounds of 2.7, 3.6, 4.5, and 5.4 Å for NOESY spectra acquired at 60 ms mixing time or 3, 4, 5, and 6 Å otherwise; all lower bounds were set to 1.8 Å. A 3D ^{13}C-filtered, ^{13}C-edited NOESY (τ_m = 100 ms) spectrum was acquired to identify intermolecular NOEs between PAH2 and SID (Zwahlen et al., 1997).

Seventy-three ϕ and seventy-three ψ constraints were derived from an analysis of H^α, C^α, C^β, C', and backbone amide nitrogen

chemical shifts using TALOS (Cornilescu et al., 1999). These constraints were applied to only those residues with reliability scores of at least 10 (for PAH2) and at least 9 (for SID). Lower and upper bounds for these constraints were set to three times the standard deviation of the predicted ϕ and ψ values. Fifty-two χ^1 torsion angle constraints were derived from the measured $^3J_{NH^\beta}$, $^3J_{H^\alpha H^\beta}$, $^3J_{NC^\gamma}$, and $^3J_{C'C^\gamma}$ values (Archer et al., 1991; Vuister et al., 1993; Grzesiek et al., 1995). In addition, 72 $^3J_{H^N H^\alpha}$ coupling constants measured from a 3D HNHA experiment were directly used for structure refinements (Kuboniwa et al., 1994).

Initial structures for the PAH2–SID complex were calculated using distance and torsion angle constraints using the program DYANA (Güntert et al., 1997). Fifty structures starting with random torsion angles were computed by minimizing the violations of the input conformational constraints via simulated annealing and torsion angle dynamics. Twenty-five structures with target functions <1 were selected for further refinement using CNS (Brünger et al., 1998). Refinements were performed using the *anneal.inp* task file. Simulated annealing in Cartesian space consisted of 5 picoseconds (ps) of equilibration at 5000 K followed by 15 ps of cooling to 0 K. This was followed by 1000 steps of constrained, conjugate gradient minimization. Force constants for the distance, torsion angle, and coupling constant constraints were scaled up to 100 kcal mol^{-1} Å^{-2}, 200 kcal mol^{-1} rad^{-2} and 1 kcal mol^{-1} Hz^{-2} during the equilibration stage and maintained at those values during the remaining stages of the refinement. For distance constraints, r^{-6} averaging was used throughout the refinement (Fletcher et al., 1996). No hydrogen bonding constraints were imposed during any stage of structure determination. Fourteen structures (56% success rate) that best satisfied the experimental constraints and simultaneously exhibited favorable Lennard-Jones potentials along with the energy-minimized average structure were selected for structural analysis.

Structures were analyzed using PROCHECK (Laskowski et al., 1996), PROMOTIF (Hutchinson, and Thornton, 1996), HBPLUS (McDonald, and Thornton, 1994), and in-house software. Structural similarity searches were performed using DALI or TOP web servers. The interfacial surface areas were computed using the MSMS program (Sanner et al., 1996). Images were generated using MOLSCRIPT (Kraulis, 1991) and RASTER3D (Merritt et al., 1997), or GRASP (Nicholls et al., 1991).

GST-Pulldown Assays

Wild-type and mutant mSin3A proteins were expressed in vitro from the *myc*-tagged pCS2MT vector using the TNT SP6 reticulocyte lysate kit (Promega) in the presence of ^{35}[S]-methionine according to the manufacturer's instructions. Glutathione S-transferase (GST) fusion proteins were expressed in *E. coli* DH5α and purified using glutathione Sepharose beads (Amersham). ^{35}S-labeled proteins were incubated with GST-SID (residues 1–27 of Mad1) in NETN buffer (20 mM Tris [pH 8.0], 1 mM EDTA, 150 mM NaCl, and 0.5% Nonidet P-40). Samples were incubated for 3 hr and then washed three times in the same buffer. The bound proteins were separated on 10% SDS-polyacrylamide gels and visualized by fluorography.

Acknowledgments

We thank Stephanie Wang, Kathleen Ratcliff, and Dr. Kanti Thirumoorthy for assistance and discussions. We also thank Dr. Barry Honig and Dr. Xiang Li for generously providing copies of GRASP and XPKASGN, respectively. This work was supported by funds from the Searle Leadership Fund (I. R.) and grants from the NIH (to R. N. E. and D. E. A.). R. N. E. is an American Cancer Society Research Professor. Funds for upgrading the 600 MHz NMR spectrometer at Northwestern were provided in part by the NIH. We gratefully acknowledge the use of instruments in the Keck Biophysics Facility at Northwestern (www.biochem.northwestern.edu/Keck/keckmain.html).

Received September 20, 2000; revised October 13, 2000.

References

Ahringer, J. (2000). NuRD and Sin3 histone deacetylase complexes in development. Trends Genet. *16*, 351–356.

Alland, L., Muhle, R., Hou, H., Potes, J., Chin, L., Schreiber-Agus, N., and DePinho, R.A. (1997). Role for N-CoR and histone deacetylase in Sin3-mediated transcriptional repression. Nature *387*, 49–55.

Archer, S.J., Ikura, M., Torchia, D.A., and Bax, A. (1991). An alternative 3D NMR technique for correlating backbone ^{15}N with side chain H$^\beta$ resonances in larger proteins. J. Magn. Reson. *95*, 636–641.

Ayer, D.E. (1999). Histone deacetylases: transcriptional repression with SINers and NuRDs. Trends Cell. Biol. *9*, 193–198.

Ayer, D.A., Lawrence, Q.A., and Eisenman, R.N. (1995). Mad-Max transcriptional repression is mediated by ternary complex formation with mammalian homologs of yeast repressor Sin3. Cell *80*, 767–776.

Ayer, D.E., Laherty, C.D., Lawrence, Q.A., Armstrong, A.P., and Eisenman, R.N. (1996). Mad proteins contain a dominant transcription repression domain. Mol. Cell. Biol. *16*, 5772–5781.

Bax, A., and Grzesiek, S. (1993). Methodological advances in protein NMR. Acc. Chem. Res. *26*, 131–138.

Berk, A. (1999). Activation of RNA polymerase II transcription. Curr. Opin. Cell Biol. *11*, 330–335.

Brünger, A.T., Adams, P.D., Clore, G.M., DeLano, W.L., Gros, P., Grosse-Kunstleve, R.W., Jiang, J.-S., Kuszewski, J., Nilges, N., Pannu, N.S., et al. (1998). Crystallography and NMR system (CNS): A new software system for macromolecular structure determination. Acta Crystallog. *D54*, 905–921.

Chen, J.D., and Evans, R.M. (1995). A transcriptional corepressor that interacts with nuclear hormone receptors. Nature *377*, 454–457.

Clore, G.M., and Gronenborn, A.M. (1994). Multidimensional heteronuclear nuclear magnetic resonance of proteins. Meth. Enzymol. *239*, 349–363.

Cornilescu, G., Delaglio, F., and Ad Bax, A. (1999). Protein backbone angle restraints from searching a database for chemical shift and sequence homology. J. Biomol. NMR *13*, 289–302.

David, G., Alland, L., Hong, S.H., Wong, C.W., DePinho, R.A., and Dejean, A. (1998). Histone deacetylase associated with mSin3A mediates repression by the acute promyelocytic leukemia-associated PLZF protein. Oncogene *14*, 2549–2556.

Dhalluin, C., Carlson, J.E., Zeng, L., He, C., Aggarwal, A.K., and Zhou, M.M. (1999). Structure and ligand of a histone acetyltransferase bromodomain. Nature *399*, 491–496.

Eilers, A.L., Billin, A.N., Liu, J., and Ayer, D.J. (1999). A 13-amino acid amphipathic α-helix is required for the functional interaction between the transcriptional repressor Mad1 and mSin3A. J. Biol. Chem. *274*, 32750–32756.

Farrow, N.A., Muhandiram, R., Singer, A.U., Pascal, S.M., Kay, C.M., Gish, G., Shoelson, S.E., Pawson, R., Forman-Kay, J.D., and Kay, L.E. (1994). Backbone dynamics of a free and a phosphopeptide-complexed Src homology domain studied by ^{15}N NMR relaxation. Biochemistry *33*, 5984–6003.

Fletcher, C.M., Jones, D.N.M., Diamond, R., and Neuhaus, D. (1996). Treatment of NOE constraints involving equivalent or non-stereoassigned protons in calculations of biomacromolecular structures. J. Biomol. NMR *8*, 292–310.

Grimes, J.A., Nielsen, S.J., Barragliol, E., Miska, E.A., Speh, J.C., Berry, D.L., Atouf, F., Holdener, B.C., Mandel, G., and Kouzarides, T. (2000). The corepressor mSin3A is a functional component of the REST-CoREST repressor complex. J. Biol. Chem. *275*, 9461–9467.

Grzesiek, S., Kuboniwa, H., Hinck, A.P., and Bax, A. (1995). Multiple-quantum line narrowing for measurement of H$^\alpha$-H$^\beta$ *J* couplings in isotopically enriched proteins. J. Am. Chem. Soc. *117*, 5312–5315.

Güntert, P., Mumenthaler, C., and Wüthrich, K. (1997). Torsion angle dynamics for NMR structure calculation with the new program DYANA. J. Mol. Biol. *273*, 283–298.

Hassig, C.A., Fleischer, T.C., Billin, A.N., Schreiber, S.L., and Ayer, D.E. (1997). Histone deacetylase activity is required for full transcription repression by mSin3A. Cell *89*, 341–347.

Heinzel, T., Lavinsky, R.M., Mullen, T.-M., Söderström, M., Laherty, C.D., Torchia, J., Yang, W.-M., Brard, G., Ngo, S.D., Davie, J.R., et al. (1997). A complex containing N-CoR, mSin3 and histone deacetylase mediates transcriptional repression. Nature *387*, 43–48.

Holm, L., and Sander, C. (1996). Mapping the protein universe. Science *273*, 595–602.

Hörlein, A.J., Näär, A.M., Heinzel, T., Torchia, J., Gloss, B., Kurokawa, R., Ryan, A., Kamei, Y., Söderström, M., Glass, C.K., and Rosenfeld, M.G. (1995). Ligand-independent repression by the thyroid hormone receptor mediated by a nuclear receptor corepressor. Nature *377*, 397–404.

Hurlin, P.J., Quéva, C., and Eisenman, R.N. (1997). Mnt, a novel Max-interacting protein is coexpressed with Myc in proliferating cells and mediates repression at Myc binding sites. Genes Dev. *11*, 44–58.

Hutchinson, E.G., and Thornton, J.M. (1996). PROMOTIF—a program to identify and analyze structural motifs in proteins. Protein Sci. *5*, 212–220.

Jacobson, R.H., Ladurner, A.G., King, D.S., and Tjian, R. (2000). Structure and function of a human $TAF_{II}250$ double bromodomain module. Science *288*, 1422–1425.

Jones, P.L., Veenstra, G.J., Wade, P.A., Vermaak, D., Kass, S.U., Landsberger, N., Strouboulis, J., and Wolffe, A.P. (1998). Methylated DNA and MeCP2 recruit histone deacetylase to repress transcription. Nat. Genet. *19*, 187–191.

Knoepfler, P.S., and Eisenman, R.N. (1999). Sin meets NuRD and other tails of repression. Cell *99*, 447–450.

Koipally, J., Renold, A., Kim, J., and Georgopoulos, K. (1999). Repression by Ikaros and Aiolos is mediated through histone deacetylase complexes. EMBO J. *18*, 3090–3100.

Kraulis, P.J. (1991). MOLSCRIPT: a program to produce both detailed and schematic plots of protein structures. J. Appl. Crystallog. *24*, 946–950.

Kuboniwa, H., Grzesiek, S., Delaglio, F., and Bax, A. (1994). Measurement of H^N-H^α J couplings in calcium-free calmodulin using new 2D and 3D water-flip-back methods. J. Biomol. NMR *4*, 871–878.

Laherty, C.D., Yang, W.-M., Sun, J.-M., Davie, J.R., Seto, E., and Eisenman, R.N. (1997). Histone deacetylases associated with the Sin3 corepressor mediate Mad transcriptional repression. Cell *89*, 349–356.

Laherty, C.D., Billin, A.N., Lavinsky, R.M., Yochum, G., Bush, A.C., Sun, J.-M., Mullen, T.-M., Davie, J.R., Rose, D.W., Glass, C.K., et al. (1998). SAP30, a component of the mSin3 corepressor complex involved in N-CoR-mediated repression by specific transcription factors. Mol. Cell *2*, 33–42.

Laskowski, R.A., Rullmann, J.A.C., MacArthur, M.W., Kaptein, R., and Thornton, J.M. (1996). AQUA and PROCHECK-NMR: Programs for checking the quality of protein structures solved by NMR. J. Biomol. NMR *8*, 477–486.

Löhr, F., and Rüterjans, H. (1996). Novel pulse sequences for the resonance assignment of aromatic side chains in ^{13}C-labeled proteins. J. Magn. Reson. Series B. *112*, 259–268.

Mathews, F.S., Levine, M., and Argos, P. (1972). Three-dimensional Fourier synthesis of calf liver cytochrome b_5 at 2.8 Å resolution. J. Mol. Biol. *64*, 449–464.

McDonald, I.K., and Thornton, J.M. (1994). Satisfying hydrogen bonding potential in proteins. J. Mol. Biol. *238*, 777–793.

Merritt, E.A., and Bacon, D.J. (1997). Raster3D: photorealistic molecular graphics. Meth. Enzymol. *277*, 505–524.

Murphy, M., Ahn, J., Walker, K.K., Hoffman, W.H., Evans, R.M., Levine, A.J., and George, D.L. (1999). Transcriptional repression by wild-type p53 utilizes histone deacetylases, mediated by interaction with mSin3A. Genes Dev. *13*, 2490–2501.

Murzin, A.G., Brenner, S.E., Hubbard, T., and Chothia, C. (1995). SCOP: a structural classification of proteins database for the investigation of sequences and structures. J. Mol. Biol. *247*, 536–540.

Nagy, L., Kao, H.-Y., Chakravarti, D., Lin, R.J., Hassig, C.A., Ayer, D.E., Scheriber, S.L., and Evans, R.M. (1997). Nuclear receptor repression mediated by a complex containing SMRT, mSin3A, and histone deacetylase. Cell *89*, 373–380.

Nan, X., Ng, H.H., Johnson, C.A., Laherty, C.D., Turner, B.M., Eisenman, R.N., and Bird, A. (1998). Transcriptional repression by the methyl-CpG-binding protein MeCP2 involves a histone deacetylase complex. Nature *393*, 386–389.

Naruse, Y., Aoki, T., Kojima, T., and Mori, N. (1999). Neural restrictive silencer factor recruits mSin3 and histone deacetylase complex to repress neuron-specific target genes. Proc. Natl. Acad. Sci. USA *96*, 13691–13696.

Ng, H.H., and Bird, A. (2000). Histone deacetylases: silencers for hire. Trends Biochem. Sci. *25*, 121–126.

Nicholls, A., Sharp, K.A., and Honig, B. (1991). Protein folding and association: insights from the interfacial and thermodynamic properties of hydrocarbons. Proteins *11*, 281–296.

Nomura, T., Khan, M.M., Kaul, S.C., Dong, H.D., Wadhwa, R., Colmenares, C., Kohno, I., and Ishii, S. (1999). Ski is a component of the histone deacetylase complex required for transcriptional repression by Mad and thyroid hormone receptor. Genes Dev. *13*, 412–423.

O'Shea, E.K., Lumb, K.J., and Kim, P.S. (1993). Peptide velcrodesign of a heterodimeric coiled-coil. Curr. Biol. *3*, 658–667.

Otting, G., and Wüthrich, K. (1990). Heteronuclear filters in two-dimensional [^{1}H,^{1}H]-NMR spectroscopy: combined use with isotope labelling for studies of macromolecular conformation and intermolecular interactions. Quart. Rev. Biophys. *23*, 39–96.

Ptashne, M., and Gann, A. (1997). Transcriptional activation by recruitment. Nature *386*, 569–577.

Radhakrishnan, I., Pérez-Alvarado, G.C., Parker, D., Dyson, H.J., Montminy, M.R., and Wright, P.E. (1999). Structural analyses of CREB-CBP transcriptional activator-coactivator complexes by NMR spectroscopy: implications for the mapping of structural domains. J. Mol. Biol. *287*, 859–865.

Sanner, M.F., Olson, A.J., and Sphener, J.-C. (1996). Reduced surface: an efficient way to compute molecular surfaces. Biopolymers *38*, 305–320.

Schreiber-Agus, N., Chin, L., Chen, K., Torres, R., Rao, G., Guida, P., Skoultchi, A.I., and DePinho, R.A. (1995). An amino-terminal domain of Mxi1 mediates anti-Myc oncogenic activity and interacts with a homolog of the yeast transcriptional repressor Sin3. Cell *80*, 777–786.

Vuister, G.W., Wang, A.C., and Bax, A. (1993). Measurement of three-bond nitrogen-carbon *J* couplings in proteins uniformly enriched in ^{15}N and ^{13}C. J. Am. Chem. Soc. *115*, 5334–5335.

Wang, J., Clark, I., Nicholson, P.R., Herskowitz, I., and Stillman, D.J. (1990). The *Saccharomyces cerevisiae SIN3* gene, a negative regulator of *HO*, contains four paired amphipathic helix motifs. Mol. Cell. Biol. *10*, 5927–5936.

Yamazaki, T., Forman-Kay, J.D., and Kay, L.E. (1993). Two-dimensional NMR experiments for correlating $^{13}C\beta$ and $^1H\delta/\epsilon$ chemical shifts of aromatic residues in ^{13}C-labeled proteins via scalar couplings. J. Am. Chem. Soc. *115*, 11054–11055.

Yang, Q., Kong, Y., Rothermel, B., Garry, D.J., Bassel-Duby, R., and Williams, R.S. (2000). The winged-helix/forkhead protein myocyte nuclear factor β (MNF-β) forms a corepressor complex with mammalian Sin3B. Biochem. J. *345*, 335–343.

Zhang, Y., Iratni, R., Erdjument-Bromage, H., Tempst, P., and Reinberg, D. (1997). Histone deacetylases and SAP18, a novel polypeptide, are components of a human Sin3 complex. Cell *89*, 357–364.

Zwahlen, C., Legault, P., Vincent, S.J.F., Greenblatt, J., Konrat, R., and Kay, L.E. (1997). Methods for measurement of intermolecular NOEs by multinuclear NMR spectroscopy: application to a bacteriophage λ N-peptide/*boxB* RNA complex. J. Am. Chem. Soc. *119*, 6711–6721.

RCSB Protein Data Bank Accession Code

The coordinates for the fourteen final structures and the average minimized structure have been deposited in the Protein Data Bank with accession code 1G1E.